



Diffraction characteristics of radiated tilted fiber grating and its spectrometer application

QINGGUO SONG,¹ YUZE DAI,¹ XIANGPENG XIAO,¹ QIZHEN SUN,¹
KAIMING ZHOU,² LIN ZHANG,² AND ZHIJUN YAN^{1,*}

¹The School of Optical and Electronic Information and Wuhan National Laboratory for Optoelectronics, Huazhong University of Science and Technology, Wuhan 430074, China

²Aston Institute of Photonic Technologies, Aston University, Birmingham B4 7ET, UK

*yanzhijun@gmail.com

Abstract: We have numerically and experimentally presented the diffraction characteristics of radiated tilted fiber grating (RTFG) in terms of the spectrum, bandwidth, degree of polarization, angular dispersion, and temperature crosstalk. The theoretical and experimental results have shown that the polarization property, bandwidth, and dispersion of RTFG highly depended on the tilt angle of RTFG, and the RTFG has ultra-low temperature crosstalk. We have simulated the transmission spectrum of the RTFG with different tilt angles (25°, 31°, 38°, 45°, and 54°), in which the results show that the larger tilt angle has the wider bandwidth. The RTFGs with the tilt angle of 25°, 31°, 38°, 45°, and 54° have the 3dB bandwidth of 110 nm, 144 nm, 182 nm, 242 nm, and 301 nm, respectively. Besides, the degree of polarization (DOP) of the radiated light from RTFG with the different tilt angles are 0.876, 0.944, 0.967, 0.998, and 0.970, respectively, and the RTFG has the maximum DOP at the tilt angle of 45°, which could be used as single-polarization diffraction device. The experimental results show that with further increase or decrease of the tilt angle, the DOP of radiated light of RTFG would decrease. Both the theoretical and experimental results show that the smaller tilt angle could greatly improve the diffraction angular dispersion of RTFG, in which the 25°, 31°, 38°, and 45° RTFG have the angular dispersion of 0.2288 °/nm, 0.1026 °/nm, 0.0714 °/nm, and 0.0528 °/nm, respectively. Due to the broad working bandwidth, the diffraction angles of RTFG have ultra-low temperature crosstalk, where -0.00042, -0.00054, -0.00064, and -0.00099 degree / °C at the tilt angle of 25°, 31°, 38°, and 45°. Finally, we have demonstrated a miniaturized spectrometer integrated by a 25° RTFG, which has a high spectral resolution of 0.08 nm. The proposed RTFG would be an ideal in-fiber diffraction device and widely applied in spectral analysis, space optical communication, and Lidar areas.

© 2022 Optica Publishing Group under the terms of the [Optica Open Access Publishing Agreement](#)

1. Introduction

In-fiber devices have compact structure and low insertion loss, which are easily integrated into optical fiber communication [1,2], optical fiber sensing [3,4] and fiber laser systems [5,6]. There are various in-fiber devices according to the different structures and functions, including fiber interferometer [7], fiber coupler [8], fiber polarizer [9], fiber sensor [10], and so on. So far, most in-fiber devices are usually used for the seamlessly integrated coupling inside the optical fiber system, in which the light is bounded inside the fiber without any external power exchange. With the rapid development of integrated optics, the coupling between the optical fiber system and free space or on-chip system has attracted more and more attention. There are several types of optical fiber devices that could couple the transmission light out of fiber in a specific direction, such as the optical fiber micro-lens [11] and angled fiber [12], and so on, which play an important role in the coupling between fiber systems and free-space systems such as optical space and on-chip systems [13]. Miniaturization and integration are the trends in the development of optical systems and devices, which is necessary to develop new types of in-fiber devices and realize the light coupling inside and outside the optical fiber system. Tilted fiber grating (TFG) has been widely

used in optical fiber sensing, fiber laser and fiber communication fields, due to its unique mode conversion property between fiber core mode, fiber cladding mode and radiation mode [14]. The TFG with a tilt angle of less than 23.1° , could couple the core mode into the backward cladding mode, in which there are a series of cladding mode resonance peaks in the transmission spectrum [15]. And for the TFG with a larger than 66.9° tilt angle, the core mode will be coupled into the forward cladding mode [16]. Especially, when the tilt angle is between 23.1° and 66.9° , the core mode will be radiated out of fiber and diffracted into free space with the wavelength-dependent radiation angle [17,18]. Due to the unique radiation and diffraction characteristics, the TFGs with a tilt angle between 23.1° and 66.9° are called radiated tilted fiber grating (RTFG) [19]. At present, the researches on RTFG are focusing on the tilt angle of 45° , which has a strong polarization dependence and the radiation direction nearly perpendicular to the fiber axis. The 45° RTFG has been proposed as the high extinction ratio in-fiber polarizer [20] or in-fiber dispersive element applying in spectral coded imaging, wireless optical communication, and linear polarization spectrometer [21–24]. Besides, the theoretical analysis has presented that RTFGs with smaller tilt angles have a larger angular dispersion [17], which is well suited as an in-fiber diffraction grating with high spectral resolution. However, the researches on the diffraction characteristics of the RTFG were only proposed in rough theoretical analysis. The RTFG has been studied in recent years, however, there are few papers to systematically reported the diffraction characteristics of RTFG, which is significant for understanding and optimizing the devices dependent on the predictability and control of the diffracted light.

2. Diffraction characteristics of RTFG

Due to the asymmetric inclined structure inside of the fiber core, the RTFG can radiate out the core mode from the fiber with a wavelength-dependent angle. In our previous works, the coupling coefficient between core mode and radiation mode was obtained by dividing the grating into sections [19]. However, the coupling coefficient of the single grating section is estimated roughly, which is inaccurate in the quantitative calculation. In this paper, we theoretically analyzed the coupling coefficient by calculating the power of incident light and radiated light.

As shown in Fig. 1, the coupling coefficient α_R of a single sub-section can be expressed as:

$$\alpha_R = \frac{P_{out}}{P_{in}} \quad (1)$$

where P_O is the power of light radiated out from one sub-section, which is the integration of the power-flow density vector S_{out} [15] out of a single sub-section. P_{in} is the power of light passing through a single sub-section, which is the integration of the power density of transmission light S_{in} inside the single sub-section. The S_{out} and S_{in} can be expressed as:

$$P_{out} = \oint S_{out} = \int_0^{2\pi} S_{out} \cdot r \cdot \delta z d\phi$$

$$= \frac{\pi \varepsilon_0 n^2 \delta n^2 k_0^3 c E_0^2}{4} \int_0^{2\pi} \left[\left(\frac{\Delta^2}{k_0^2 n_0^2} + \frac{k_t^2}{k_0^2 n_0^2} \right)^2 \sin^2(\delta - \phi) \right] \cdot F(\phi)^2 d\phi \quad (2)$$

$$P_{in} = \oint S_{in} = \int_0^{2\pi} \int_0^r S_{in} dr d\phi = \pi n \sqrt{\frac{\varepsilon_0}{\mu_0}} \int_0^a J_0(ur)^2 E_0^2 dr \quad (3)$$

where ε_0 and μ_0 are the dielectric constant and permeability. $k_0 = 2\pi/\lambda$ is the wave vector of the incident light, n is the effective refractive index of core mode. δn is the modulated refractive index. E_0 is the intensity of the electric field. ϕ is the radial angle. r is the radius of the circular surface of a single sub-section. δz is the axial length of a single sub-section, which is half of the radial period Λ of the 45° RTFG. $\Delta = \beta - K_g$ is the detuning between the wavenumber of the incident light and the wavevector of the optical fiber grating. $k_t = \sqrt{k_0^2 n_0^2 - \Delta^2}$ is the transverse

component of the wave vector for the radiated light. δ is the degree of polarization of incident light. F is given:

$$F = \left[\frac{K_s J_0(ua) J_1(K_s a) - u J_1(ua) J_0(K_s a)}{K_s^2 - u^2} \right] \quad (4)$$

where $K_s = \sqrt{k_t^2 + K_l^2 + 2k_t K_l \sin\phi}$, $K_l = 2\pi \sin\theta_G / \Lambda_G$ and $K_g = 2\pi \cos\theta_G / \Lambda_G$ are the transverse and longitudinal wavenumbers of the optical fiber grating. a is the radius of the fiber core. Thus, the α_R will be:

$$\alpha_R = \frac{\epsilon_0^{1/2} \mu_0^{1/2} n^3 \delta n^2 k_0^3 c E_0}{4} \cdot \frac{\int_0^{2\pi} \left[\left(\frac{\Delta^2}{k_0^2 n_0^2} + \frac{k_t^2}{k_0^2 n_0^2} \right)^2 \sin^2(\delta - \phi) \right] F(\phi)^2 d\phi}{\int_0^a J_0(ur)^2 dr} \quad (5)$$

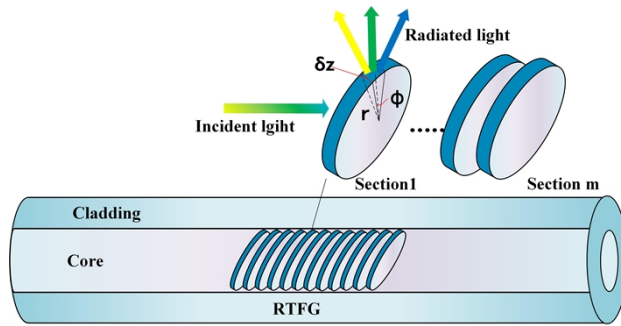


Fig. 1. The diffraction characteristics of RTFG.

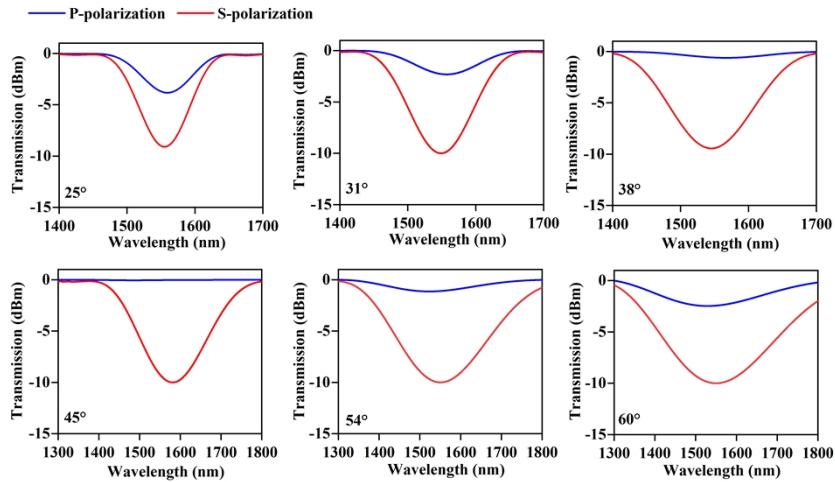


Fig. 2. The simulated transmission spectrum at the tilt angles of 25°, 31°, 38°, 45°, 54°, and 60°.

The coupling coefficient α of RTFG can be expressed as:

$$\alpha = \alpha_R (1 - \alpha_R)^m \quad (6)$$

where m is the number of sub-sections, which is the ratio of optical fiber grating L to period Λ .

According to Eqs. (1–6), the transmission spectrums of RTFG with different tilt angles (25° , 31° , 38° , 45° , 54° , and 60°) are simulated, in which the grating period of each RTFG with different tilt angles is set as 593 nm, 623 nm, 680 nm, 778 nm, 930 nm, 1092 nm, corresponding to a radiated central wavelength of 1550 nm (seen in Fig. 2), which is clearly shown that the RTFG has the maximum polarization dependent loss (PDL) when the tilt angle is 45° .

The transmission spectrum of RTFG with the tilt angles of 25° , 31° , 38° , 45° , and 54° are experimentally measured, as shown in Fig. 3, which is highly consistent with the simulation. In particular, when the tilt angle is 25° , the cladding mode and radiation mode exist simultaneously around the wavelength of 1550 nm by chance. By immersing the RTFG into the index-matching liquid, the cladding mode can be eliminated. And for the RTFGs with other tilt angles, the cladding mode is far from 1550 nm so that the transmission spectrum only contains radiation mode.

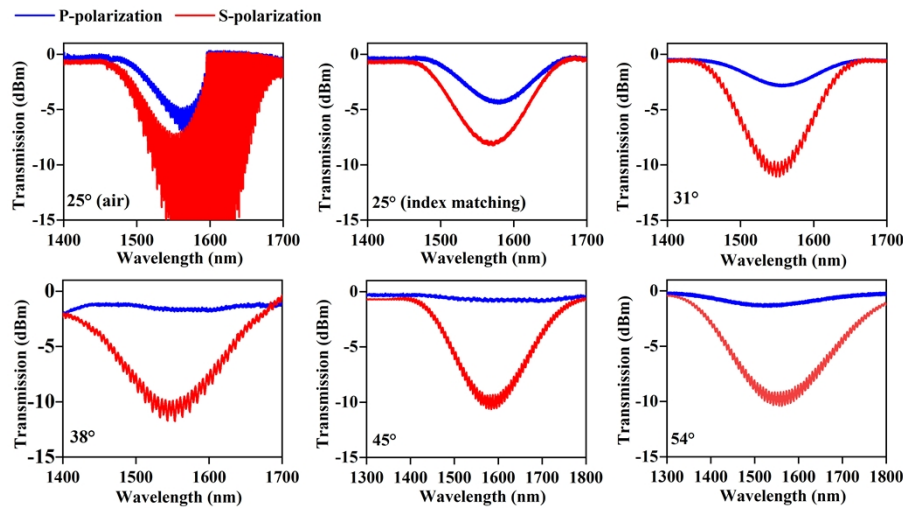


Fig. 3. The measured transmission spectrum at the tilt angles of 25° , 31° , 38° , 45° , and 54° .

The central wavelength of RTFG in which the radiation mode has the strongest coupling efficient is governed by the phase match condition [17]:

$$\lambda_c = n\Lambda_z(1 + \cos 2\theta) = 2n\Lambda_G \cos\theta. \quad (7)$$

Figures 4(a) and (b) show the relationship between the central wavelength and tilt angle, grating period. The experimental results are consistent with the simulation results very well.

The simulated and measured transmission spectra of the RTFG with different tilt angles show various spectral characteristics. The further analysis of the spectral bandwidth is carried out by the transmission spectrum at S-polarization in terms of tilt angle and radiation intensity. Figures 5(a) and (b) illustrate the 3dB-bandwidth of RTFG versus to the different tilt angle and coupling efficient of radiation mode at the central wavelength of RTFG, in which the RTFG with a larger tilt angle and higher coupling efficient has the broader 3dB-bandwidth.

In our previous works, the radiated light from the 45° RTFG has a degree of polarization (DOP) higher than 0.99, which can be regarded as linearly polarized light. However, for the RTFG with other tilt angles, the radiated light is partially polarized. To investigate the DOP of RTFG with different tilt angles, we have designed the experimental setup, seen in Fig. 6(a), in which an unpolarized light is from an amplified spontaneous emission (ASE) source, and radiated by the RTFG of a certain tilt angle (25° , 31° , 38° , and 45°). The partially polarized light is from

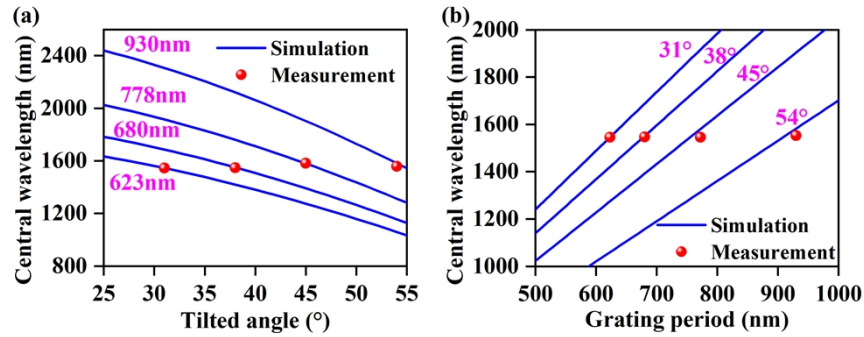


Fig. 4. The central wavelength to (a) tilt angle and (b) grating period by the analytical methods of phase match condition and measurement.

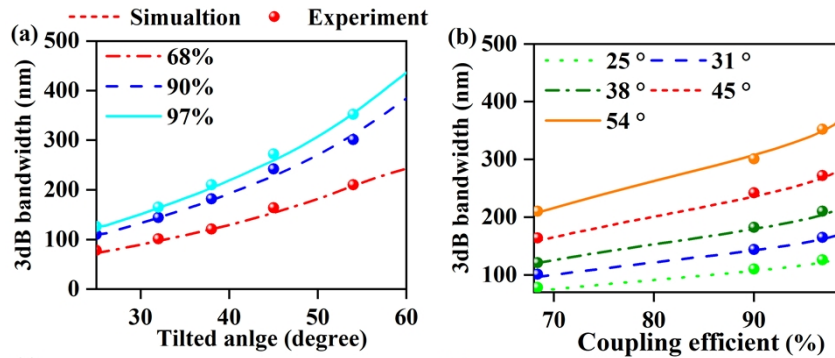


Fig. 5. The 3dB-bandwidth to (a) the tilt angle and (b) coupling efficient at the central wavelength of RTFG.

the RTFG through a rotatable polarizer that can change the polarization angle and is received by the power meter. By adjusting the polarization angle of the rotatable polarizer, the maximum and minimum powers of radiated light are recorded (P_{max} and P_{min}), which corresponds to the power of the whole partially polarized light and the unpolarized light, respectively. The DOP can be calculated by: $DOP = 1 - P_{min}/P_{max}$ [17]. The experimental result is shown in Fig. 7 (b), in which the DOP of 25°, 31°, 38°, 45°, and 54° are 0.876, 0.944, 0.967, 0.998, and 0.970, respectively. The DOP of radiated light of RTFG is the maximum at the tilt angle of 45°, which is because the 45° is the Brewster’s angle of optical fiber grating and radiated light would be purely s-polarized [18].

The 45° RTFG has the ability of both polarizing and diffraction to disperse the in-fiber transmission light into free space. However, the dispersion of 45° RTFG is proposed of ~ 0.053 °/nm, which is not suited for the field with a demand for high spectral resolution. According to previous theoretical analysis, the RTFGs with small tilt angles have high angular dispersion. The diffraction angle of the radiation mode can be expressed as:

$$\cos\gamma = \frac{\Delta}{k_0 n_0} = \frac{\Lambda\beta - 2\pi\cos\theta}{\Lambda k_0 n_0}. \quad (8)$$

According to Eq. (8), we have numerically analyzed the angular dispersion characteristic of RTFG with different tilt angles. As shown in Fig. 7(a), the RTFG with a smaller tilt angle has the larger angular dispersion, and the RTFG with a larger tilt angle has the better dispersion linearity. Figure 7(b) shows the relationship between the angular dispersion and tilt angle at

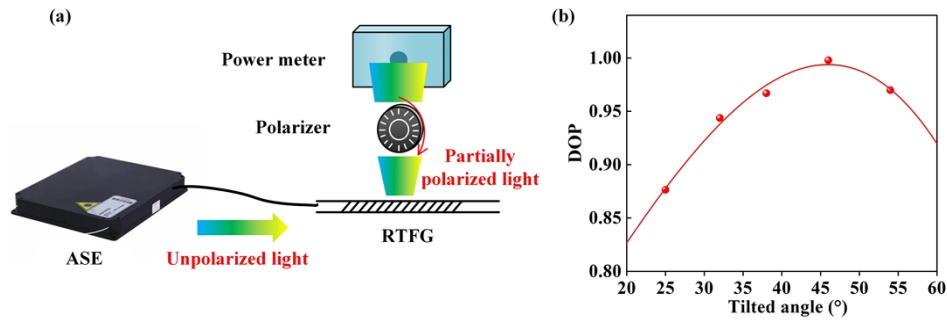


Fig. 6. (a) Experimental set up for DOP. (b) The DOP of the light radiated from RTFG with different tilt angles.

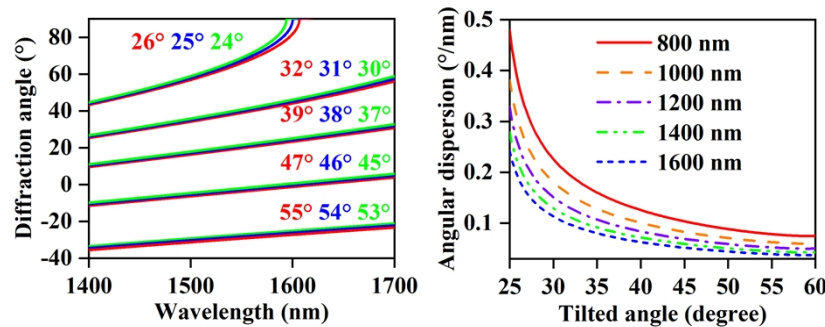


Fig. 7. (a) Simulation of the dispersion characteristic at different tilt angles. (b) Simulation of angular dispersion to tilt angle of RTFG at different radiated central wavelengths.

the different radiated central wavelengths, in which the angular dispersion is decreasing as the central wavelength increases.

To verify the simulation results, we measured the angular dispersion of RTFG at different tilt angles. The central wavelength of the radiated mode is set to cover 1500 nm to 1600 nm, which well matches the wavelength range of the light source and detector. Therefore, four groups of RTFGs are fabricated using the phase mask with different periods, which all have a central wavelength between 1500 nm and 1600 nm. The tilt angle and period parameters of RTFGs are given in Table 1.

The angular dispersion measurement system is illustrated in Fig. 8(a), in which an array detector is used to record the position of the radiation light. By moving the array detector and recording the position change of the radiation light, the diffraction angle γ of RTFG can be get, which is expressed as:

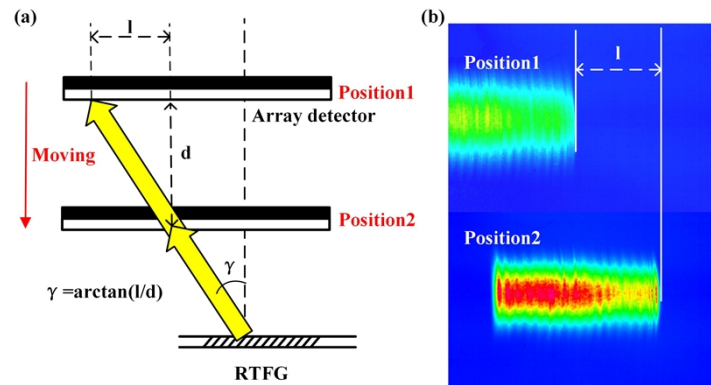
$$\gamma = \arctan(l/d) \quad (9)$$

where d is the displacement of the array detector and l is the position change of the radiation light. Figure 9(b) shows the light image before and after moving the array detector, where the position change of the beam is measured.

As shown in Fig. 9, the dispersion curves at the tilt angle of 24°, 25°, and 26° are not linear. To compare the angular dispersion of RTFG, the points near the central wavelength of 1550 nm are selected for linear fitting, in which the angular dispersions are 0.2446 °/nm, 0.2288 °/nm, and 0.215 °/nm. And for the other curves at the higher tilt angles (31°, 38°, 45°), the angular dispersion is measured of 0.1026 °/nm, 0.0714 °/nm, 0.0528 °/nm, respectively. The angular dispersion of RTFG is decreasing as increasing of the tilt angle.

Table 1. The tilt angle and period parameters of RTFG

Group	Tilt angle (°)	Period (nm)	Central wavelength (nm)
1	24	596	1575
	25	593	1555
	26	591	1536
2	30	625	1569
	31	623	1545
	32	620	1520
3	37	684	1577
	38	680	1547
	39	676	1515
4	45	778	1582
	46	772	1545
	47	767	1505

**Fig. 8.** (a) Dispersion measurement system; (b) the image before and after moving the array detector.

For most optical fiber devices, temperature crosstalk is a very important parameter. In the experiment, we have measured the temperature response of the diffraction angle at different tilt angles (25° , 31° , 38° , 45°). As shown in Fig. 10, the temperature is stepwise increased from 10°C to 110°C with an increment of 10°C by the temperature controlling system, and the wavelength of diffracted light is set as 1550 nm , which is the central wavelength. The increased temperature led to the increase of the effective refractive index of core mode n_0 , which would cause the decrease of diffraction angle according to Eq. (10). The temperature crosstalk of the diffraction angle is -0.00042 , -0.00054 , -0.00064 , and -0.00099 at the tilt angle of 25° , 31° , 38° , and 45° , respectively. The experimental results show that the RTFG has low-temperature crosstalk, which can work as a temperature-insensitive diffractive fiber device.

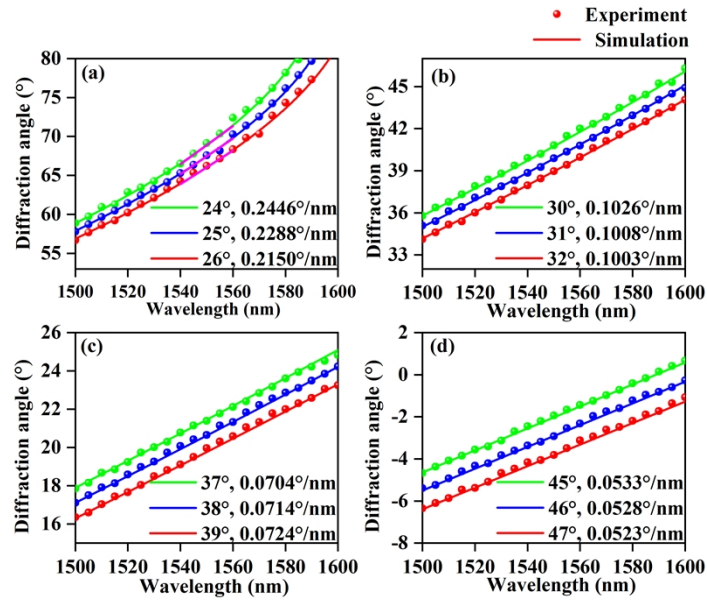


Fig. 9. Measured angular dispersion of RTFG at different tilt angles of (a) 24°, 25°, 26°; (b) 31°, 32°, 33°; (c) 37°, 38°, 39°; (d) 45°, 46°, 47°.

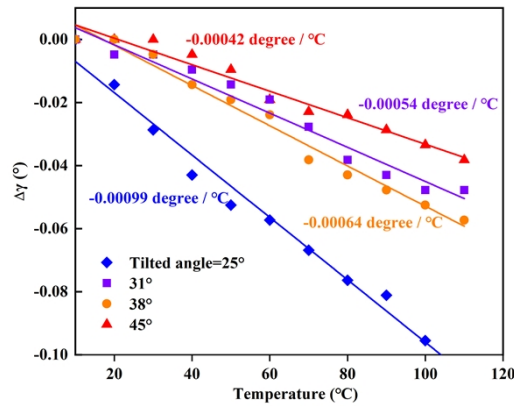


Fig. 10. The temperature response of the diffraction angle at the tilt angle of 25°, 31°, 38°, and 45°

3. Spectrometer application of RTFG

The RTFG shows a good performance in light diffraction, which could be potentially applied in spectral analysis. In previous research, the in-fiber spectrometers based on TFG with a very small tilt angle have been reported [25]. However, for TFG with a small tilt angle, the fiber core mode would be coupled into cladding mode and has a very weak leak mode. For the application of the spectrometer, to eliminate the effect of the cladding mode, the grating must be immersed in the index-matching liquid or attached with a prism to couple the cladding mode into radiation mode, which limits the miniaturization of the spectrometer. Based on the above analysis of RTFG, the 25° RTFG has a better dispersion capability which can couple the light directly out of the fiber without index-matching and with a higher angular dispersion. In this section, we demonstrated a miniaturized spectrometer with a high resolution by using the 25° RTFG as an in-fiber dispersion device. The schematic diagram of the miniaturized spectrometer based on 25° RTFG is given in Fig. 11(a), in which a cylindrical lens with a 150 mm focal distance is used to focus the diffraction light with the same wavelength from different positions of the grating into several pixels of the array detector. A mirror is used to fold the optical path to reduce the footprint of the spectrometer system. The associated experimental setup is given in Fig. 11(b), in which a tunable laser is used to measure the spectral response. Figure 11(c) shows the spectral response by sweeping the tunable laser from 1538 nm to 1559 nm with a wavelength increment of 1 nm where 22 clear spectral peaks can be identified, and the difference in light intensity at each wavelength is caused by the spectral response of array detector and the slight inaccuracy of collimated optical path. The line dispersion is shown in Fig. 11(d), in which the dispersion curves provide great linearity of 569.918 $\mu\text{m}/\text{nm}$, corresponding to a high spectral resolution of 0.08 nm. In the previous report, the in-fiber spectrometer employed a 45° RTFG has a spectral resolution of 0.3 nm [24]. In contrast, the resolution is increased by four times by replacing the 45° RTFG with the 25° RTFG. Furthermore, according to the temperature crosstalk of the diffraction angle which is -0.00042 degree /°C (seen in Fig. 10), when the external temperature changes by 1°C, the wavelength will have a drift of 0.001 nm.

To evaluate the performance of the miniaturized spectrometer based on 25° RTFG, we fabricate a fiber Bragg grating (FBG) array demodulation system, as shown in Fig. 12(a), where a broadband ASE source and a circulator are applied, the reflected light from the circulator port 3 is divided into two beams of equal energy by a coupler, and detected by the proposed miniaturized spectrometer and a commercial optical spectrum analyzer (YOKOGAWA) with a resolution of 0.05 nm, respectively. As shown in Fig. 12(b), the spectral shape measured by the proposed miniaturized spectrometer nicely overlaps the one captured by the commercial OSA, confirming its decent spectral analysis performance, and the power discrepancies at some wavelength range are mainly caused by the wavelength-dependent responsivity of the detector array which can be mitigated after calibration.

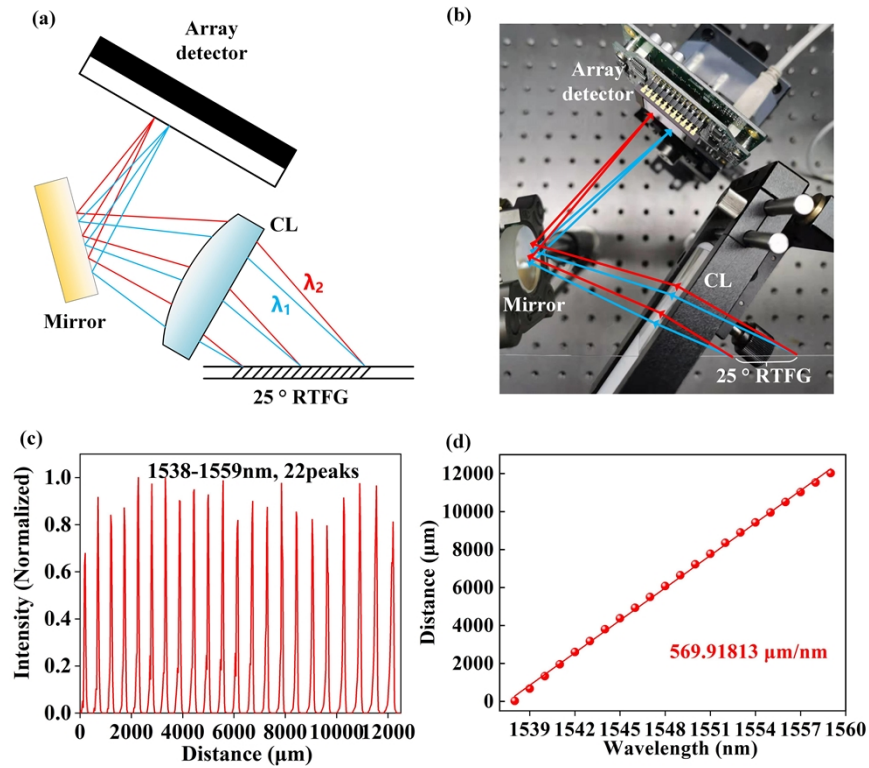


Fig. 11. The miniaturized spectrometer based on 25° RTFG. (a) Schematic diagram. (b) Experimental setup photo. (c) Measured spectral response. (d) Line dispersion curve.

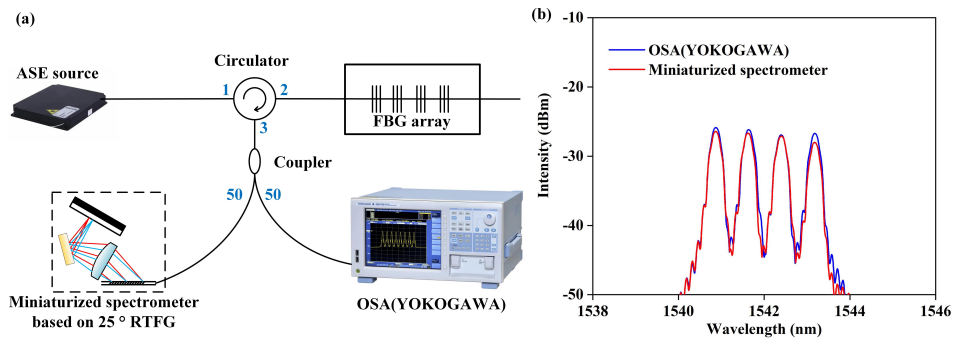


Fig. 12. (a) FBG demodulation system for evaluating the performance of the miniaturized spectrometer based on 25° RTFG. (b) Reflection spectrum of FBG array detected by proposed miniaturized spectrometer and OSA.

4. Conclusion

In conclusion, we have theoretically and experimentally investigated the diffraction characteristics of RTFG, in which the spectral bandwidth, DOP and angular dispersion of RTFG with different tilt angles and periods have been discussed in both theory and experiment. By using the UV-phase mask inscription method, a series of RTFGs with a tilt angle of 25°, 31°, 38°, 45°, and 54° are fabricated to verify the theoretical analysis. The results have shown that the RTFG with a larger tilt angle has a wider working bandwidth. The radiated light of RTFG with a 45° tilt angle has a maximum DOP of 0.998. And the RTFG with the tilt angle of 25°, 31°, 38°, and 45° show the angular dispersion of 0.2288 °/nm, 0.1026 °/nm, 0.0714 °/nm, and 0.0528 °/nm, respectively. Furthermore, The temperature crosstalk testing results show the RTFG shows very low-temperature crosstalk, which is -0.00042, -0.00054, -0.00064, and -0.00099 for the RTFG with the tilt angle of 25°, 31°, 38°, and 45°, respectively. Finally, we have demonstrated a 25° RTFG-based miniaturized spectrometer, which has a spectral resolution of 0.08 nm.

Funding. National Natural Science Foundation of China (62075071); National Science Fund for Distinguished Young Scholars (61922033).

Disclosures. The authors declare no conflicts of interest.

Data availability. Data underlying the results presented in this paper are not publicly available at this time but may be obtained from the authors upon reasonable request.

References

1. B. J. Puttnam, G. Rademacher, and R. S. Luís, "Space-division multiplexing for optical fiber communications," *Optica* **8**(9), 1186–1203 (2021).
2. Y. Liu, R. Guo, J. Zhao, P. Chen, Y. Gu, Y. Ning, Y. You, and X. Chou, "An EDFA-Gain Equalizer Based On a Sagnac Loop With an Unpumped Erbium-Doped Fiber," *J. Lightwave Technol.* **39**(13), 4496–4502 (2021).
3. S. Yuezheng, Y. Zhijun, Z. Kaiming, L. Binbin, J. Biqiang, M. Chengbo, S. Qizhen, and Z. Lin, "Excessively Tilted Fiber Grating Sensors," *J. Lightwave Technol.* **39**(12), 3761–3770 (2021).
4. J. He, J. He, X. Xu, B. Du, B. Xu, C. Liao, Z. Bai, and Y. Wang, "Single-mode helical Bragg grating waveguide created in a multimode coreless fiber by femtosecond laser direct writing," *Photonics Res.* **9**(10), 2052–2059 (2021).
5. D. Wang, Y. Jiang, X. Geng, B. Yang, and L. Li, "Study of asymmetric biconical fiber tapers for in-fiber Mach-Zehnder interferometers and applications in single-frequency fiber lasers," *Opt. Express* **29**(10), 14384–14393 (2021).
6. Y. Wang, S. Hou, Y. Yu, W. Liu, P. Yan, and J. Yang, "Photonic device combined optical microfiber coupler with saturable-absorption materials and its application in mode-locked fiber laser," *Opt. Express* **29**(13), 20526–20534 (2021).
7. W. Lin, L. Y. Shao, M. I. Vai, P. P. Shum, S. Liu, Y. Liu, F. Zhao, D. Xiao, Y. Liu, Y. Tan, and W. Wang, "In-Fiber Mach-Zehnder Interferometer Sensor Based on Er Doped Fiber Peanut Structure in Fiber Ring Laser," *J. Lightwave Technol.* **39**(10), 3350–3357 (2021).
8. G. Pelegriña-Bonilla, K. Hausmann, H. Tünnermann, P. Weßels, H. Sayinc, U. Morgner, J. Neumann, and D. Kracht, "Analysis of the Coupling Mechanism in Asymmetric Fused Fiber Couplers," *J. Lightwave Technol.* **32**(13), 2382–2391 (2014).
9. X. Zhang, C. Wang, R. Yu, L. Xiao, X.-S. Zhu, and Y.-W. Shi, "Fiber polarizer based on selectively silver-coated large-core suspended-core fiber," *Opt. Lett.* **46**(10), 2429–2432 (2021).
10. Q. Ma, L. Li, F. Wei, J. Sun, F. Yu, J. Huang, X. Gu, and Y. Ma, "High sensitivity sensors based on open cavity in-fiber Fabry-Perot and Mach-Zehnder interferometers," *J. Opt. Technol.* **88**(1), 37–41 (2021).
11. S.-B. Wen, V. M. Sundaram, D. McBride, and Y. Yang, "Low-cost, high-precision micro-lensed optical fiber providing deep-micrometer to deep-nanometer-level light focusing," *Opt. Lett.* **41**(8), 1793–1796 (2016).
12. X. Liu and J. U. Kang, "Optimization of an angled fiber probe for common-path optical coherence tomography," *Opt. Lett.* **38**(15), 2660–2662 (2013).
13. J. M. Ward, F. Lei, S. Vincent, P. Gupta, S. K. Mondal, J. Fick, and S. Nic Chormaic, "Excitation of whispering gallery modes with a "point-and-play," fiber-based, optical nano-antenna," *Opt. Lett.* **44**(13), 3386–3389 (2019).
14. T. Erdogan and J. E. Sipe, "Tilted fiber phase gratings," *J. Opt. Soc. Am. A* **13**(2), 296–313 (1996).
15. Z. Li, X. Ruan, and Y. Dai, "Leaky Mode Combs in Tilted Fiber Bragg Grating," *J. Lightwave Technol.* **37**(24), 6165–6173 (2019).
16. Z. Yan, H. Wang, C. Wang, Z. Sun, G. Yin, K. Zhou, Y. Wang, W. Zhao, and L. Zhang, "Theoretical and experimental analysis of excessively tilted fiber gratings," *Opt. Express* **24**(11), 12107–12115 (2016).
17. Y. Li, M. Froggatt, and T. Erdogan, "Volume Current Method for Analysis of Tilted Fiber Gratings," *J. Lightwave Technol.* **19**(10), 1580–1591 (2001).
18. Z. Yan, C. Mou, K. Zhou, X. Chen, and L. Zhang, "UV-Inscription, Polarization-Dependant Loss Characteristics and Applications of 45° Tilted Fiber Gratings," *J. Lightwave Technol.* **29**(18), 2715–2724 (2011).

19. H. Qin, Q. He, Z. Xing, X. Guo, Z. Yan, Q. Sun, K. Zhou, H. Wang, D. Liu, and L. Zhang, "Numerical and Experimental Characterization of Radiation Mode of 45° Tilted Fiber Grating," *J. Lightwave Technol.* **37**(15), 1 (2019).
20. K. Zhou, G. Simpson, X. Chen, L. Zhang, and I. Bennion, "High extinction ratio in-fiber polarizers based on 45° tilted fiber Bragg gratings," *Opt. Lett.* **30**(11), 1285–1287 (2005).
21. G. Wang, C. Wang, Z. Yan, and L. Zhang, "Highly efficient spectrally encoded imaging using a 45° tilted fiber grating," *Opt. Lett.* **41**(11), 2398–2401 (2016).
22. G. Wang, U. Habib, Z. Yan, N. J. Gomes, Q. Sui, J.-B. Wang, L. Zhang, and C. Wang, "Highly Efficient Optical Beam Steering Using an In-Fiber Diffraction Grating for Full Duplex Indoor Optical Wireless Communication," *J. Lightwave Technol.* **36**(19), 4618–4625 (2018).
23. H. Qin, Q. He, Z. Xing, X. Guo, Z. Yan, Q. Sun, C. Wang, K. Zhou, D. Liu, and L. Zhang, "In-fiber single-polarization diffraction grating based on radiant tilted fiber grating," *Opt. Lett.* **44**(17), 4407–4410 (2019).
24. H. Qin, Q. He, Y. Moreno, Z. Xing, X. Guo, Z. Yan, Q. Sun, K. Zhou, D. Liu, and L. Zhang, "Compact linear polarization spectrometer based on radiation mode shaped in-fiber diffraction grating," *Opt. Lett.* **44**(21), 5129–5132 (2019).
25. J. L. Wagener, T. A. Strasser, J. R. Pedrazzani, J. DeMarco, and D. DiGiovanni, "Fiber grating optical spectrum analyzer tap," in *11th International Conference on Integrated Optics and Optical Fibre Communications and 23rd European Conference on Optical Communications* 5, 65–68 (1997).